SIMULATION OF PHYSICAL PROCESSES

Original article
DOI: https://doi.org/10.18721/JPM.15303

COMPARATIVE EVALUATION OF RANS EDDY-VISCOSITY TURBULENCE MODELS FOR CALCULATING THE SILICON MELT CONVECTION IN CRYSTAL GROWTH SYSTEMS

D. V. Borisov✉, *V. V. Kalaev*

STR Group, Inc. – Soft-Impact, Ltd., St. Petersburg, Russia

✉ dmitriy.borisov@str-soft.com

Abstract. In the paper, the results of RANS calculations of turbulent convection in silicon melt, obtained using several eddy-viscosity turbulence models, have been compared with previously published ILES eddy-resolving calculation data for similar conditions. A turbulence model was chosen for its subsequent problem-oriented modification with the algebraic introduction of factors that could produce the required anisotropy of the Reynolds stress tensor and the turbulent heat flux vector including in the Reynolds-averaged equations of momentum and energy. As applied to the problems of calculating the convection in crystal growth furnace crucibles using the Czochralski method, it was shown the expediency of taking either the one-equation k-model or the two-equation k-ε model as the initial RANS-model for modification.

Keywords: Czochralski method, ILES, RANS, Reynolds stress tensor, turbulent heat transfer

Citation: Borisov D. V., Kalaev V. V., Comparative evaluation of RANS eddy-viscosity turbulence models for calculating the silicon melt convection in crystal growth systems, St. Petersburg Polytechnical State University Journal. Physics and Mathematics. 15 (3) (2022) 28–42. DOI: https://doi.org/10.18721/JPM.15303

Научная статья
УДК 532.5
DOI: https://doi.org/10.18721/JPM.15303

СРАВНИТЕЛЬНАЯ ОЦЕНКА RANS-МОДЕЛЕЙ ТУРБУЛЕНТНОСТИ С ИЗОТРОПНОЙ ВЯЗКОСТЬЮ ДЛЯ РАСЧЕТА КОНВЕКЦИИ РАСПЛАВА КРЕМНИЯ В УСТАНОВКАХ ВЫРАЩИВАНИЯ КРИСТАЛЛОВ

Д. В. Борисов✉, *В. В. Калаев*

АО «Группа СТР» – ООО «Софт-Импакт», Санкт-Петербург, Россия

✉ dmitriy.borisov@str-soft.com

Аннотация. В работе сопоставляются результаты RANS-расчетов турбулентной конвекции в расплаве кремния, полученные по нескольким моделям турбулентности с изотропной вязкостью, с ранее опубликованными данными вихреразрешающих ILES-вычислений для аналогичных условий. Выбирается модель турбулентности для ее последующей проблемно-ориентированной модификации с алгебраическим введением факторов, которые могут продуцировать нужную анизотропию тензора Рейнольдсовых напряжений и вектора турбулентного теплового потока, входящих в осредненные по Рейнольдсу уравнения движения и энергии. Показано, что применительно к задачам расчета конвекции в тиглях установок, где используют метод Чохральского, целесообразно взять для модификации либо однопараметрическую k-модель, либо двухпараметрическую k-ε модель в качестве исходной RANS-модели.

Ключевые слова: метод Чохральского, ILES, RANS, тензор Рейнольдсовых напряжений, турбулентный теплоперенос, конвекция

Ссылка для цитирования: Борисов Д. В., Калаев В. В. Сравнительная оценка RANS-моделей турбулентности с изотропной вязкостью для расчета конвекции расплава кремния в установках выращивания кристаллов // Научно-технические ведомости СПбГПУ. Физико-математические науки. 2022. Т. 15. № 3. С. 28–42. DOI: https://doi.org/10.18721/JPM.15303

Introduction

The Czochralski method is one of the main techniques for producing semiconductor silicon crystals, widely used in the electronics industry [1–3]. High-quality can be achieved in single crystals by controlling the mass transfer of impurities in the melt that are assimilated into the crystal during the growth process. As a rule, the flow of silicon melt is turbulent, which is due to the growing conditions even for crystals with a relatively small diameter (10 cm) in laboratory systems. The presence of turbulent structures with different sizes in crucibles for industrial growth of crystals of 20–30 cm in diameter makes it difficult to control the concentration of impurities; it can also trigger a transition from monocrystalline to polycrystalline growth [4]. Experimental studies into turbulent flow of silicon melt are hindered by both high temperatures of the processes and the requirements imposed on the precision of the equipment used to measure turbulent fluctuations. In view of this, numerical modeling seems to be the most promising method for studying turbulent flow and the processes of heat and mass transfer in silicon melt.

The most accurate method for computations of turbulent flows is direct numerical simulation (DNS), aimed at resolving all spatio-temporal scales of turbulence without resorting to additional hypotheses to close equations [2, 3]. However, this method requires significant computational resources, making it impossible to use in practical engineering calculations. The most popular and relatively economical approach is based on Reynolds-averaged Navier–Stokes equations (RANS), allowing, in particular, to perform computations in an axisymmetric formulation.

The k-ε turbulence model was adopted in [5] to numerically study the effect of crucible rotation on heat transfer in silicon melt based on the RANS approach. The computational results showed a general qualitative agreement with the experimental data. The computations in [6] were performed using a low-Reynolds-number k-ε model, finding, in particular, enhanced heat and mass transfer with an increase in the crucible rotation rate. Similar results could not be achieved with previous computations assuming laminar convection, which did not involve any turbulence model. The computed distributions for the melt temperature and the interface shape also yielded good agreement with the experimental data. Three turbulence models were tested in [7] to calculate turbulent convection in the melt: the 'standard' k-ε model using near-wall functions; the two-layer k-ε model combined with the one-equation model near solid boundaries; the Launder–Jones low-Reynolds-number k-ε model [8]. An apparent advantage detected for the third model was that it could to produce solutions close to laminar ones for weakened turbulence. Turbulent characteristics of silicon melt in an idealized cylindrical crucible were considered in [9] using the unsteady RANS (URANS) approach in a three-dimensional formulation. The computations adopted the Launder–Sharma k-ε model [10], as well as Menter's k-ω SST model [11, 12]. These URANS computations confirm the advantage of the SST model, providing the best resolution of the flow structure and near-wall temperature gradients, as well as generating more intense flow on the free surface of the melt.

Numerical modeling of silicon melt convection in industrial crucibles (by the Czochralski method) based on axisymmetric RANS formulation met with moderate success. However, a number of important characteristics of heat and mass transfer in the melt could not be reproduced within this approach. For example, to correctly model the thermal stresses and point defects in the crystal volume, it is necessary to accurately predict the shape of the crystallization front, which largely depends on the flow structure and heat transfer in the melt. For instance, the experimental and calculated curvatures of the interfaces obtained in [13–16] in simulations of heat transfer in the melt by the RANS approach differed by 2–3 times. The key reason for this discrepancy for crystals with a diameter of 100 mm is that RANS computations predict strong downward flow in the vicinity of the crucible's symmetry axis, which is not observed experimentally [17]. Modifications were introduced in [16] to the RANS turbulence model to more accurately predict the shape of the crystallization front in simulations of the growth processes for crystals 300 mm in diameter, produced by the Czochralski method. However, the authors specify that these modifications were introduced to artificially overcome the particular deficiency of the RANS turbulence model in the region below the crystal rather than improve the model itself.

Another important characteristic of convection in the silicon melt that affects the properties and quality of the crystal is the oxygen concentration in the melt. The results obtained in early attempts to use the RANS turbulence model to predict the level of oxygen concentration in a wide range of parameters controlling the operation of a Czochralski furnace were inconsistent with the experimental data [6, 18].

Most RANS models are based on the Boussinesq hypothesis assuming isotropic turbulent viscosity, and on the standard gradient diffusion hypothesis (SGDH) closing Reynolds-averaged equations for transport of temperature.

We investigated the local applicability of the Boussinesq and SGDH hypotheses to simulations of the Reynolds stress tensor and the turbulent heat flux vector in silicon melt in our previous study [19]. For this purpose, we used a specialized technique to process and analyze the results of computations based on the implicit eddy-resolving method (ILES). Furthermore, it was found that the strong anisotropy of the Reynolds stress tensor in the vicinity of the crucible wall, the crystallization interface and free surface of the melt is not reproduced by the Boussinesq hypothesis; the latter was exclusively designed to describe shear stresses. In addition, pronounced anisotropy of turbulent heat transfer near the free surface is also not described within the SGDH hypothesis.

The main objectives of this study are formulated as follows:

compare the results of RANS computations of turbulent convection in silicon melt, obtained by several turbulence models with isotropic viscosity, with the data obtained based on the ILES approach, published earlier in [19];

select RANS turbulence models for subsequent modification with adjustments introduced based on the data from ILES computations.

The results of RANS computations of conjugate heat transfer presented in this paper were obtained with the Flow Module software package, which is part of the CGSim code developed by the STR Group for simulation of heat and mass transfer during crystal growth by various methods [20].

We used the following low-Reynolds-number turbulence models: Wolfshtein k-model [21]; Chien k-ε model [22]; Menter k-ω SST model [11, 12].

Using the Flow Module and ANSYS Fluent packages for the Menter model, we also conducted cross-verification for a simplified problem, simulating turbulent convection in the melt only.

Mathematical model

Numerical modeling for growing silicon crystals by the Czochralski method includes turbulent convection and heat transfer in the melt and in inert gas (argon) circulated above the melt. Thermal conductivity is computed in quartz and graphite crucibles, as well as in silicon single crystal. The mathematical model based on the RANS approach incorporates steady-state equations for mass, momentum and temperature balance:

$$\nabla\cdot\left(\rho\overline{\mathbf{u}}\right)=0, \tag{1}$$

$$\nabla\cdot\left(\rho\overline{\mathbf{u}}\overline{\mathbf{u}}\right)=-\nabla\overline{p}+\nabla\cdot\left(\boldsymbol{\tau}-\rho\overline{\mathbf{u}'\mathbf{u}'}\right)+\left(\rho-\rho_0\right)\mathbf{g}, \tag{2}$$

$$\boldsymbol{\tau}=\mu\left(\nabla\overline{\mathbf{u}}+\left(\nabla\overline{\mathbf{u}}\right)^T\right)-\frac{2}{3}\mu\left(\nabla\cdot\overline{\mathbf{u}}\right)\mathbf{E}, \tag{3}$$

$$\nabla\cdot\left(\rho c_p\overline{\mathbf{u}T}\right)=\nabla\cdot\left(\lambda\nabla\overline{T}-\rho c_p\overline{\mathbf{u}'T'}\right), \tag{4}$$

$$\rho=\begin{cases}\rho\left(T\right), & \text{for melt or solid region}\\ \dfrac{p_0M}{R_gT}, & \text{for gas,}\end{cases} \tag{5}$$

Here ρ, ρ_0, kg/m^3, are the local and steady-state densities, respectively; **u,** m/s, is the velocity vector; p, p_0, Pa, are the local pressure and the gas pressure in the furnace, respectively; **g** is the gravitational acceleration; τ is the viscous stress tensor, **E** is the unit tensor; μ, Pa·s, is the dynamic viscosity; c_p, J/(kg·K), is the specific heat capacity at constant pressure; T, K, is the temperature, λ, W/(m·K), is the thermal conductivity; M, amu, is the molecular weight; R_g, J/(kmol·K), is the universal gas constant.

The overbar denotes Reynolds averaging of the quantity, the prime corresponds to a fluctuating component; $\overline{\mathbf{u}'\mathbf{u}'}$ and $\overline{\mathbf{u}'T'}$ denote the Reynolds stress tensor and the turbulent heat flux vector, respectively.

Turbulent transport of momentum and heat is simulated assuming turbulent eddy viscosity and SGDH:

$$\overline{\mathbf{u}'\mathbf{u}'}=\frac{2}{3}k\mathbf{E}-\nu_t\left(\nabla\overline{\mathbf{u}}+\left(\nabla\overline{\mathbf{u}}\right)^T-\frac{2}{3}\left(\nabla\cdot\overline{\mathbf{u}}\right)\mathbf{E}\right); \tag{6}$$

$$\overline{\mathbf{u}'T'}=-\frac{\nu_t}{\mathrm{Pr}_t}\nabla\overline{T}, \tag{7}$$

where ν_t m^2/s, is the kinematic turbulent viscosity, determined in accordance with the turbulence model; Pr_t is the turbulent Prandtl number.

System of equations (1)–(5) is complemented with one or two equations for transport: turbulent kinetic energy k, m^2/s^2 (for all models used), dissipation rate ε, m^2/s^3 (for Chien's model) and specific dissipation rate ω, 1/s (for Menter's model).

According to the Wolfshtein and Chien models, turbulent viscosity is determined as follows:

$$\nu_t = C_\mu f_\mu \frac{k^2}{\varepsilon}, \tag{8}$$

where C_μ is the empirical constant, f_μ is the damping function.

According to Menter's SST model, turbulent viscosity is determined as

$$\nu_t = \frac{a_1 k}{\max\left(a_1 \omega, SF_2\right)}, \tag{9}$$

where a_1 is the model constant; S, 1/s, is the magnitude of the strain rate tensor, F_2 is the model function introduced in [11].

Computational tools

Computations of turbulent heat transfer in the melt were carried out in the two-dimensional/axisymmetrical configuration of the Flow Module package. The finite volume method was used to discretize system of equations (1)–(5). The discretized equations were solved by the SIMPLEC algorithm. The convective terms of heat flux and velocity components were approximated by the QUICK scheme, and the turbulent kinetic energy and specific dissipation were computed using a first-order upwind scheme. Diffusion fluxes were computed with second-order accuracy.

A two-dimensional/axisymmetric version of the ANSYS Fluent software package was also used in benchmark computations for the simplified model problem presented below. The SIMPLEC algorithm was used to solve the discretized equations, the convective terms in the equations for velocity components and temperature were treated by the QUICK scheme, the convective terms in the equations for k and ω were computed by a first-order upwind scheme.

Model problem

The computational domain of the model problem only covered the region of the melt (Fig. 1). The crucible radius R_c = 170 mm, the crystal radius R_s = 50 mm, the melt height H = 97 mm.

The following boundary conditions were imposed: no slip on the crucible wall and the crystallization front; zero shear stress on the free surface of the melt; temperature dependence on the radius-to-depth ratio of the melt, obtained from the experimental values [17]. The crystallization front was taken at a constant temperature equal to the melting point of silicon; the free surface was considered adiabatic.

The properties of liquid silicon used in the computations are given in Table 1. The model problem was solved without accounting for the Marangoni effect. The rotational speeds of the crucible wall ω_c and the crystal wall ω_s amounted to 5 and 20 rpm, respectively (see Fig. 1).

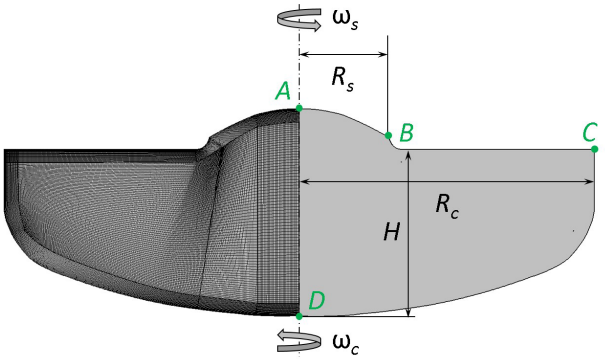

Fig. 1. Computational domain (right) and mesh (left) of the model problem:
AB is the melt/crystal interface; *BC*, *CD* are the melt/gas (free) and melt/crucible interfaces; *DA* is the axis of symmetry; R_c, R_s are the melt and crystal radii, respectively; H is the melt height; ω_c, ω_s are the angular velocities of crucible and crystal rotation, respectively

The computational mesh contained about 72,000 cells, the size of the first near-surface cell was about 0.12 mm, the size of the cell in the volume was about 1.8 mm. The dimensionless coordinate y^+ in the first near-wall cell did not exceed unity.

Fig. 2 shows a comparison of the radial temperature distributions, velocity components and turbulent viscosity for melt depths of 1 and 3 cm, obtained using Flow Module and ANSYS Fluent. Evidently, the results obtained in both packages are in good agreement. Small differences can be observed in the distributions of the axial and radial velocity components in the vicinity of the symmetry axis, which can be due to different approximations of the terms inversely proportional to the radial coordinate; the terms appear in the equation for balance of momentum written in cylindrical coordinates.

Table 1

Parameter values of liquid silicon used in the computations

Parameter	Notation	Unit	Value
Density	ρ	kg/m^3	$3{,}194–0.3701 \cdot T$
Equilibrium density	ρ_0	kg/m^3	2,570
Thermal conductivity	λ	W/(m·K)	66.5
Heat capacity	c_p	J/(kg·K)	915
Dynamic viscosity	μ	Pa·s	$8 \cdot 10^{-4}$
Melting temperature	T_m	K	1,685
Marangoni coefficient	$\partial\sigma/\partial T$	N/(m·K)	$-1 \cdot 10^{-4}$
Emissivity factor	ε_{rad}	–	0.3

Note. The data given in the last two rows will be used below.

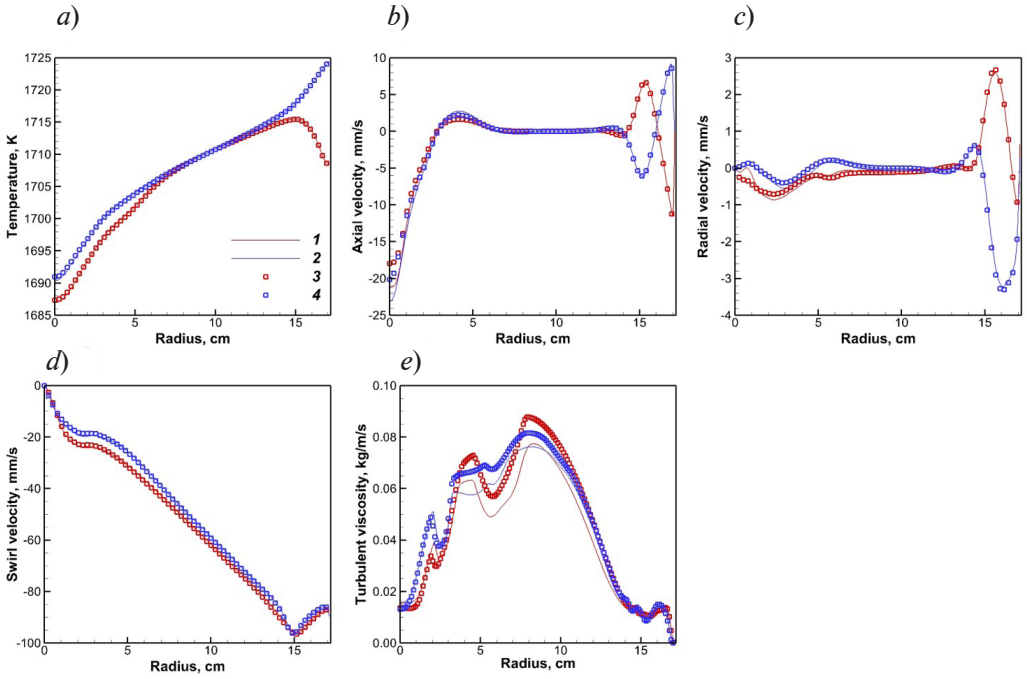

Fig. 2. Comparison of radial temperature distributions (*a*); axial (*b*), radial (*c*), circumferential (*d*) velocity components, and turbulent viscosity (*e*) computed at different melt depths: 1 cm (*1*, *3*) and 3 cm (*2*, *4*), using ANSYS Fluent (*1*, *2*) and Flow Module (*3*, *4*)

Fig. 3 compares the heat flux density distributions along the crucible wall obtained with the Flow Module and ANSYS Fluent packages. The difference between the distributions increases as it approaches the symmetry axis, which may due to the differences in the flow structure. Despite the slight discrepancy between the results obtained by both codes, we can conclude that the Menter model is implemented correctly in the Flow Module package.

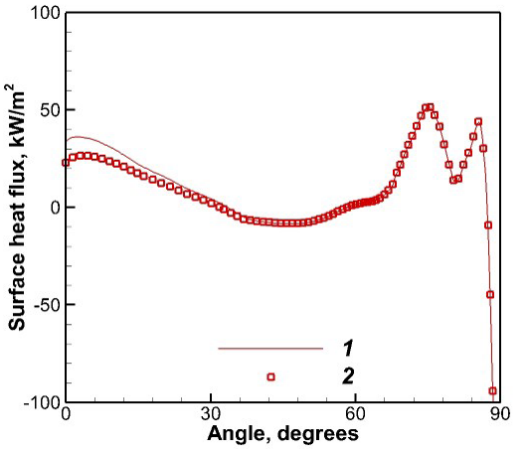

Fig. 3. Heat flux density distributions along the crucible obtained with ANSYS Fluent (*1*) and Flow Module (*2*)

Statement of the conjugate problem

The computational domain of the conjugate problem, formulated based on the data for the EKZ-1300 system [23], includes the melt, the crystal, the quartz and graphite crucibles, as well as a part of the gas region above the melt. The scheme of the computational domain is shown in Fig. 4. The crucible radius $R_c = 170$ mm, the crystal radius $R_s = 50$ mm, the melt height $H = 97$ mm.

The following boundary conditions are imposed: no slip at the melt/crucible and melt/crystal

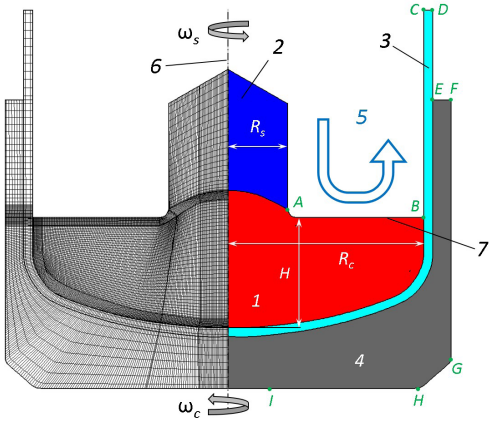

Fig. 4. Schemes of computational domain (right) and mesh (left) for the conjugate problem: melt *1*; crystal *2*; quartz and graphite crucibles *3* and *4*, respectively; argon flow *5*; symmetry axis *6*; free surface *7* (the remaining notations are the same as in Fig. 1)

interfaces, zero outlet pressure at the outlet boundary.

The boundary condition on the free surface of the melt takes into account the thermocapillary Marangoni effect:

$$\left(\mu\frac{\partial u_\tau}{\partial n}\right)_{melt} = \left(\mu\frac{\partial u_\tau}{\partial n}\right)_{gas} + \frac{\partial\sigma}{\partial T}\frac{\partial T}{\partial\tau}, \qquad (10)$$

τ corresponds to the direction tangential to the free surface, and n to the normal; the subscripts *melt* and *gas* denote the melt and the gas, respectively.

The crystallization front is maintained at a constant temperature equal to the melting point of silicon.

The following condition is imposed at the outer boundaries:

$$\left(\lambda\frac{\partial T}{\partial n}\right)_{ext} = \left(\lambda\frac{\partial T}{\partial n}\right)_{gas} + \sigma_{SB}\varepsilon_{rad}T_{ext}^4 - Q_{rad}^{in}, \qquad (11)$$

where σ_{SB} is the Stefan–Boltzmann constant; ε_{rad} is the emissivity Q_{rad}^{in} is the incident radiant heat flux obtained from the solution to the problem on global heat transfer for the EKZ-1300 system (Fig. 5); the subscript *ext* corresponds to the outer boundary, the subscript *gas* to the adjacent gas region.

A constant gas flow rate $v = 0.66$ m/s is given at the inlet boundary. The rotation rates of the crucible, ω_c, and the crystal, ω_s, amounted to 5 and 20 rpm, respectively (see Fig. 1). The properties of the materials used in the computations are given in Table 2.

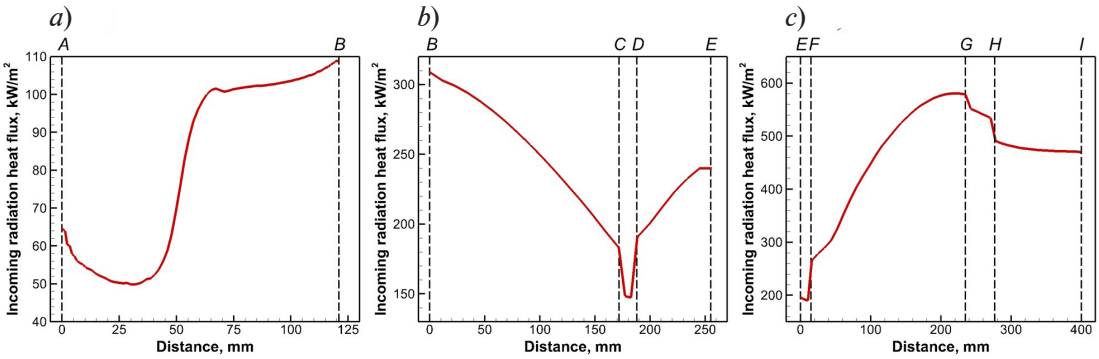

Fig. 5. Distributions of incident radiant heat flux along the free surface (*a*), along the quartz (*b*) and graphite (*c*) crucibles
Vertical dashes highlight the behavior of the curves specific to each type of crucible (see Fig. 4)

Table 2

Characteristics of substances used in the computations for the conjugate problem

Substance	Parameter value			
	ρ, kg/m^3	λ, W/(m·K)	c_p, J/(kg·K)	ε_{rad}
Solid silicon	2330	$44–0.0138\cdot T$	$687–0.236\cdot T$	$0.9016–0.00026208\cdot T$
Quartz	2650	4	1,232	0.85
Graphite	2000	$70.7–0.0191\cdot T$	2,019	0.80
Argon	$\frac{p_0 M}{R_g T}$	$0.01–2.5\cdot10^{-5}\ T$	532	–
	$\mu = 8.466\cdot10^{-6} + 5.365\cdot10^{-6}\cdot T - 8.682\cdot10^{-12}T^2$ Pa·s; $\rho_0 = 0.01$ kg/m^3; $p_0 = 3000$ Pa; $M = 40$ AU			

Note. The properties of liquid silicon are given above in Table 1.
Notations: p_0 is the gas pressure in the furnace; M is the molecular weight; the rest correspond to those given in Table 1.

The governing parameters of this problem were the Prandtl number Pr, the Grashof number Gr, the Rayleigh number Ra, the rotational Reynolds numbers Re_c (crucible) and Re_s (crystal), the Marangoni number Ma, and the number DN characterizing the influence of shear stress in gas on the melt flow along the free surface. They are defined as follows:

$$\mathrm{Pr} = \frac{\mu c_p}{\lambda} = 1.1 \cdot 10^{-2}, \tag{12}$$

$$\mathrm{Gr} = \frac{g\beta \Delta T_{bulk} H^3}{\nu^2} = 3.4 \cdot 10^8, \tag{13}$$

$$\mathrm{Ra} = \mathrm{Gr} \cdot \mathrm{Pr} = 3.7 \cdot 10^6, \tag{14}$$

$$\mathrm{Re}_c = \frac{\omega_c R_c^2}{\nu} = 4.9 \cdot 10^4, \tag{15}$$

$$\mathrm{Re}_s = \frac{\omega_s R_s^2}{\nu} = 1.7 \cdot 10^4, \tag{16}$$

$$\mathrm{Ma} = -\frac{\partial \sigma}{\partial T} \frac{H^2 \Delta T_{fs}}{L \mu a} = 6.7 \cdot 10^3, \tag{17}$$

$$\mathrm{DN} = \frac{\langle \tau_g \rangle H^2 \rho}{\mu^2} = 2.6 \cdot 10^6. \tag{18}$$

Here ΔT_{bulk} = 25.2 K is the temperature difference between the point where the crystallization front intersects the symmetry axis and the point where melt/crucible interface intersects the symmetry axis; ν, m^2/s, is the kinematic viscosity, $\nu = \mu/\rho$; ΔT_{fs} = 19.3 K is the temperature difference between the triple points corresponding to melt/gas/crystal and melt/gas/crucible; L, m, is the characteristic length of the free surface, $L = R_c - R_s$; a, m^2/s, is the thermal conductivity, $a = \nu/\mathrm{Pr}$; $\langle \tau_g \rangle$, Pa, is the average value of the gas shear stress along the free surface.

Computations were carried out on three meshes (using the Wolfshtein model) to study mesh sensitivity. The basic mesh contained about 20,000 cells, the size of the first near-surface cell was about 0.3 mm, the size of the cell in the melt was about 3.6 mm (see Fig 4). The coarse and the refined mesh were obtained by decreasing and increasing the number of cells by 2 times in each direction in the melt and by 1–2 times in the remaining blocks.

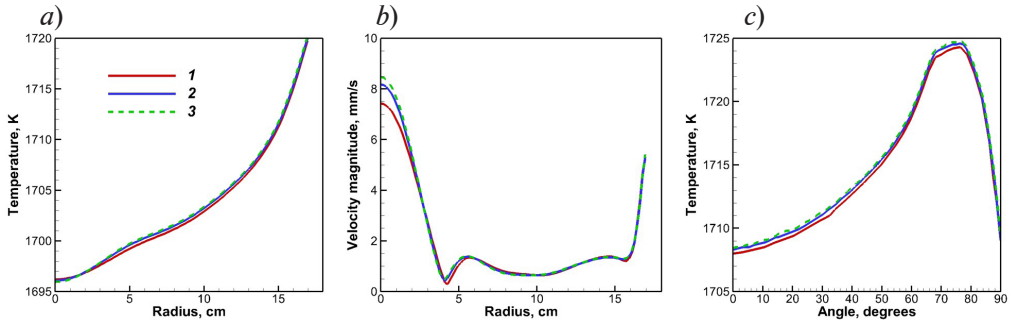

Fig. 6. Comparison of radial temperature profiles (*a*) and the magnitude of the meridional velocity component (*b*) at a depth of 2 cm from the free surface of the melt with an angular temperature distribution along the melt/crucible interface (*c*). The results obtained with coarse (*1*), basic (*2*) and refined (*3*) meshes are also compared.
Angles of 0° and 90° correspond to the points where the crucible wall intersects with the symmetry axis and the free surface of the melt, respectively

Computational results for conjugate problem

Fig. 6 shows the radial temperature profiles, the magnitude of the meridional velocity component at a depth of 2 cm from the free surface of the melt, as well as the temperature distribution along the melt/crucible interface, obtained in computations on three meshes. As can be seen from the distributions, the differences between the results obtained on the basic and the refined mesh are smaller than when between the results obtained on the coarse and the basic mesh, so we mesh convergence can be established for the computations performed. Due to the small difference between the solutions obtained on the basic and refined mesh, subsequent computations were carried out on the basic mesh.

Fig. 7 compares the temperature fields, the magnitude of the meridional velocity component, as well as the velocity vectors obtained by the ILES and RANS approaches. The temperature difference closest to the ILES data is predicted by the Wolfshtein model, while the Chien model predicts an underestimated difference, and the Menter model an overestimated one. The vortical structure in the vicinity of the crucible's vertical wall, clearly manifested in the ILES solution, is also reproduced by the models of Wolfshtein and Menter, while the Chen model predicts a different flow structure: with relatively low velocities at the edges of the melt.

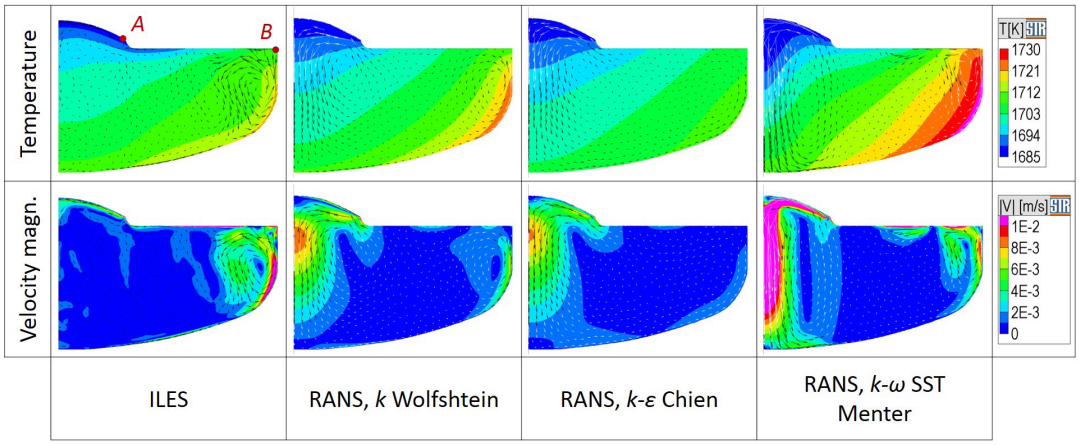

Fig. 7. Distributions of temperature (top row), magnitude of the meridional velocity component (bottom row) over the melt; vector velocity fields (marked by arrows), obtained by ILES and RANS computations based on the Wolfshtein, Chien and Menter models (from left to right)

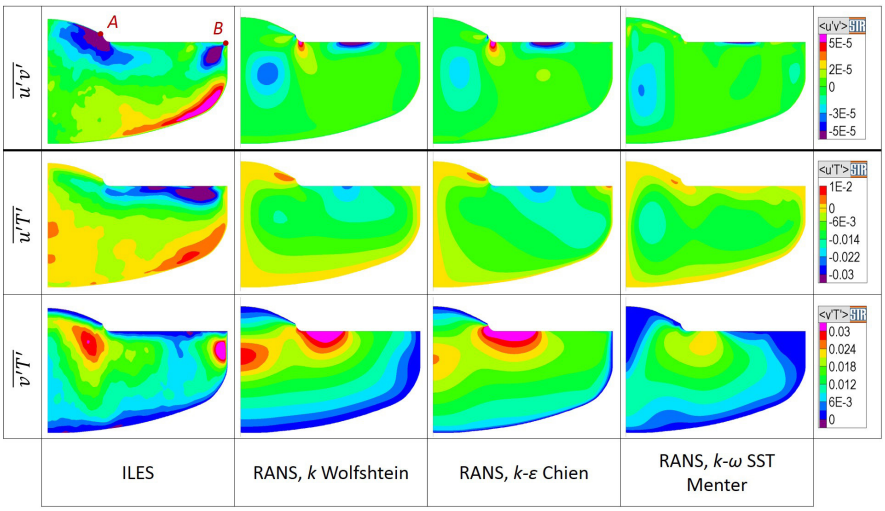

Fig. 8. Distributions of shear component $\overline{u'v'}$ of Reynolds stress tensor (top row) and components of turbulent heat flux vector (middle and bottom rows) obtained in ILES and RANS computations based on the Wolfshtein, Chien and Menter models (from left to right)

It should be noted that all turbulence models considered predict a pronounced downward flow of the melt in the vicinity of the symmetry axis, which contradicts the results of ILES computations, where high melt velocities are not observed under the crystal. The strongest downward flow is predicted by the Menter model, which also gives the lowest level of turbulent viscosity.

Fig. 8, *a* shows a comparison of the shear component $\overline{u'v'}$ of the Reynolds stress tensor obtained by ILES and RANS computations. Here u' corresponds to radial fluctuations of velocity and v' to the axial ones. Qualitative disagreement can be observed in the distributions of components $\overline{u'v'}$ predicted by ILES and RANS approaches. The highest absolute values in ILES computations $\overline{u'v'}$ are observed in the vicinity of the meniscus, near the gas/crucible/melt triple point and near the rounded part of the crucible wall. As established in [19], this feature is associated with the anisotropy of velocity fluctuations, which consists in stronger damping of normal fluctuations, compared with longitudinal fluctuations near the solid wall, as well as damping of only normal fluctuations at a free surface.

Thus, the reason for the qualitative difference in the distributions of the component $\overline{u'v'}$ in ILES and RANS computations is that the eddy viscosity assumption does not include a factor producing surface anisotropy.

Fig. 8,*b* compares the components of the turbulent heat flux vector. The ILES approach predicts the drop in the component $\overline{v'T'}$ near the horizontal part of the free surface, while high negative values are observed for the the component $\overline{u'T'}$. The average level of turbulent heat flux is consistent in ILES and RANS computations. If special modifications accounting for the effect of the free surface on turbulence are not introduced, the level of turbulent viscosity obtained on the free surface is of the same order of magnitude as in the volume of the melt. This, in turn, produces high values of both the horizontal and vertical components of the flow, which contradicts the results of ILES computations predicting pronounced anisotropy of heat transfer and attributing the decrease in the values of the component $\overline{v'T'}$ to damping of normal velocity fluctuations.

Conclusion

The results of RANS computations of turbulent convection in silicon melt obtained by several turbulence models with isotropic viscosity were compared with the data for ILES computations carried out for similar conditions.

In what concerns the temperature distributions the models of isotropic turbulent viscosity reflect the heat transfer characteristics in the melt of Czochralski furnaces for growing crystals. However, isotropic viscosity models cannot correctly account for the details of heat and mass transfer in the melt that are important for studying the influence of growth parameters in order to optimize the growing process. At the same time, we can conclude that models with two differential equations for predicting the flow structure and temperature field do not offer any advantages compared to the model with only one equation. The strongest differences in the predictions of the three RANS models for the convection structure compared to the ILES data are observed for the k-ω SST-model.

The disadvantages of RANS models with isotropic viscosity can be overcome by using models of Reynolds stress transfer, requiring to additionally solve several substantially nonlinear differential equations. However, this can lead to numerical difficulties in obtaining a steady-state solution [24]. Another approach is problem-oriented modification of the initial models of isotropic viscosity, algebraically introducing factors that, as we established in [25], can produce the required anisotropy of the Reynolds stress tensor and the turbulent heat flux vector included in the Reynolds-averaged equations of motion and energy. Comparing the results of RANS and ILES computations presented in this paper, we can conclude that either a one-parameter k-model or a two-parameter k-ε model is preferable as the initial RANS model for modification in problems dedicated to simulation of convection in the crucibles of Czochralski furnaces.

REFERENCES

1. **Vegad M., Bhatt N. M.,** Review of some aspects of single crystal growth using Czochralski crystal growth technique, Procedia Technol. 14 (2nd Int. Conf. on Innovations in Automation and Mechatronics Engin. (ICIAME 2014)) (2014) 438–446.

2. **Wagner C., Friedrich R.,** Direct numerical simulation of momentum and heat transport in idealized Czochralski crystal growth configurations, Int. J. Heat & Fluid Flow. 25 (3) (2004) 431–443.

3. **Raufeisen A., Breuer M., Botsch T., Delgado A.,** DNS of rotating buoyancy- and surface tension-driven flow, // Int. J. Heat & Mass Transfer. 51 (25–26) (2008) 6219–6234.

4. **Gräbner O., Mühe A., Müller G., et al.,** Analysis of turbulent flow in silicon melts by optical temperature measurement, Mater. Sci. Eng. B. 73 (1–3) (2000) 130–133.

5. **Kobayashi S., Miyahara S., Fujiwara T., et al.,** Turbulent heat transfer through the melt in silicon Czochralski growth, J. Cryst. Growth. 109 (1–4) (1991) 149–154.

6. **Kinney T. A., Brown R. A.,** Application of turbulence modeling to the integrated hydrodynamic thermal-capillary model of Czochralski crystal growth of silicon, J. Cryst. Growth. 132 (3–4) (1993) 551–574.

7. **Lipchin A., Brown R. A.,** Comparison of three turbulence models for simulation of melt convection in Czochralski crystal growth of silicon, J. Cryst. Growth. 205 (1–2) (1999) 71–91.

8. **Jones W. P., Launder B. E.,** The prediction of laminarization with a two-equation model of turbulence, Int. J. Heat & Mass Transfer. 15 (2) (1972) 301–314.

9. **Verma S., Dewan A.,** Thermofluid characteristics of Czochralski melt convection using 3D URANS computations, ASME J. Therm. Sci. Eng. Appl. 11 (6) (2019) 061017.

10. **Launder B. E., Sharma B. I.,** Application of the energy-dissipation model of turbulence to the calculation of flow near a spinning disc, Lett. Heat & Mass Transfer. 1 (2) (1974) 131–137.

11. **Menter F. R.** Zonal two equation k-ω turbulence models for aerodynamic flows, Proc. 24th Fluid Dynamics Conf., July 6 – 9, 1993, Orlando, Florida, USA, American Institute of Aeronautics & Astronautics (AIAA), 1993. Paper 1993–2906.

12. **Menter F. R., Kuntz M., Langtry R.,** Ten years of industrial experience with the SST turbulence model, In book: "Turbulence, Heat and Mass Transfer 4". Proc. Symp. on Turbulence, Heat & Mass Transfer. 12–17 Oct., 2003, Antalya, Turkey. Ed. by Hanjalić K., Nagano Y., Tummers M. J., Book Ser. Turbulence, Heat & Mass Transfer. Vol. 4, Begell House Inc., USA (2003) 625–632.

13. **Lipchin A., Brown R. A.,** Hybrid finite-volume/finite-element simulation of heat transfer and melt turbulence in Czochralski crystal growth of silicon, J. Cryst. Growth. 216 (1–4) (2000) 192–203.

14. **Kalaev V. V., Lukanin D. P., Zabelin V. A., et al.,** Prediction of bulk defects in CZ Si crystals using 3D unsteady calculations of melt convection, Mater. Sci. Semicond. Proc. 5 (4–5) (2002) 369–373.

15. **Kalaev V. V., Lukanin D. P, Zabelin V. A., et al.,** Calculation of bulk defects in CZ Si growth impact of melt turbulent fluctuations, J. Cryst. Growth. 250 (1–2) (2003) 203–208.

16. **Wetzel T., Virbulis J., Muiznieks A., et al.,** Prediction of the growth interface shape in industrial 300 mm CZ Si crystal growth, J. Cryst. Growth. 266 (1–3) (2004) 34–39.

17. **Gräbner O., Müller G., Virbulis J., et al.,** Effects of various magnetic field configurations on temperature distributions in Czochralski silicon melts, Microelectr. Eng. 56 (1–2) (2001) 83–88.

18. **Müller G, Mühe A., Backofen R., et al.,** Study of oxygen transport in Czochralski growth of silicon, Microelectr. Eng. 1999. Vol. 45 (2–3) (1999) 135–147.

19. **Borisov D. V., Kalaev V. V.,** ILES of melt turbulent convection with conjugated heat transfer in the crucible and gas flow for Czochralski silicon crystal growth system, J. Cryst. Growth. 573 (1 November) (2021) 126305.

20. Software package CGSim [Electronic resource]. URL: http://www.str-soft.com/products/CGSim/ (Last accessed date: March 29, 2022).

21. **Wolfshtein M.,** The velocity and temperature distribution in one-dimensional flow with turbulence augmentation and pressure gradient, Int. J. Heat & Mass Transfer. 12 (3) (1969) 301–318.

22. **Chien K.-Y.,** Predictions of channel and boundary-layer flows with a low-Reynolds number turbulence model, AIAA J. 20 (1) (1982) 33–38.

23. **Kalaev V., Sattler A., Kadinski L.,** Crystal twisting in Cz Si growth, J. Cryst. Growth. 413 (1 March) (2015) 12–16.

24. **Ristorcelli J. R., Lumley J. L.,** A second-order turbulence simulation of the Czochralski crystal growth melt: the buoyantly driven flow, J. Cryst. Growth. 129 (1–2) (1993) 249–265.

25. **Kalaev V., Borisov D., Smirnov A.,** A modified hypothesis of Reynolds stress tensor modeling for mixed turbulent convection in crystal growth, J. Cryst. Growth. 580 (15 February) (2022) 126464.

СПИСОК ЛИТЕРАТУРЫ

1. **Vegad M., Bhatt N. M.** Review of some aspects of single crystal growth using Czochralski crystal growth technique // Procedia Technology. 2014. Vol. 14. 2nd International Conference on Innovations in Automation and Mechatronics Engineering (ICIAME 2014). Pp. 438–446.

2. **Wagner C., Friedrich R.** Direct numerical simulation of momentum and heat transport in idealized Czochralski crystal growth configurations // International Journal of Heat and Fluid Flow. 2004. Vol. 25. No. 3. Pp. 431–443.

3. **Raufeisen A., Breuer M., Botsch T., Delgado A.** DNS of rotating buoyancy- and surface tension-driven flow // International Journal of Heat and Mass Transfer. 2008. Vol. 51. No. 25–26. Pp. 6219–6234.

4. **Gräbner O., Mühe A., Müller G., Tomzig E., Virbulis J., Ammon W. V.** Analysis of turbulent flow in silicon melts by optical temperature measurement // Materials Science and Engineering. B. 2000. Vol. 73. No. 1–3 Pp. 130–133.

5. **Kobayashi S., Miyahara S., Fujiwara T., Kubo T., Fujiwara H.** Turbulent heat transfer through the melt in silicon Czochralski growth // Journal of Crystal Growth. 1991. Vol. 109. No. 1–4. Pp. 149–154.

6. **Kinney T. A., Brown R. A.** Application of turbulence modeling to the integrated hydrodynamic thermal-capillary model of Czochralski crystal growth of silicon // Journal of Crystal Growth. 1993. Vol. 132. No. 3–4. Pp. 551–574.

7. **Lipchin A., Brown R. A.** Comparison of three turbulence models for simulation of melt convection in Czochralski crystal growth of silicon // Journal of Crystal Growth. 1999. Vol. 205. No. 1–2. Pp. 71–91.

8. **Jones W. P., Launder B. E.** The prediction of laminarization with a two-equation model of turbulence // International Journal of Heat and Mass Transfer. 1972. Vol. 15. No. 2. Pp. 301–314.

9. **Verma S., Dewan A**. Thermofluid characteristics of Czochralski melt convection using 3D URANS computations // ASME Journal of Thermal Science and Engineering Applications. 2019. Vol. 11. No. 6. P. 061017.

10. **Launder B. E., Sharma B. I.** Application of the energy-dissipation model of turbulence to the calculation of flow near a spinning disc // Letters in Heat and Mass Transfer. 1974. Vol. 1. No. 2. Pp. 131–137.

11. **Menter F. R.** Zonal two equation k-ω turbulence models for aerodynamic flows // Proceedings of the 24th Fluid Dynamics Conference. July 6 – 9, 1993, Orlando, Florida, USA. American Institute of Aeronautics & Astronautics (AIAA). 1993. Paper 1993–2906.

12. **Menter F. R., Kuntz M., Langtry R.** Ten years of industrial experience with the SST turbulence model // "Turbulence, Heat and Mass Transfer 4". Proceedings of the Symposium on Turbulence, Heat and Mass Transfer. 12 – 17 October, 2003. Antalya, Turkey. Ed. by Hanjalić K., Nagano Y., Tummers M. J. Book Series: Turbulence, Heat and Mass Transfer. Vol. 4. USA: Begell House Inc., 2003. Pp. 625–632.

13. **Lipchin A., Brown R. A.** Hybrid finite-volume/finite-element simulation of heat transfer and melt turbulence in Czochralski crystal growth of silicon // Journal of Crystal Growth. 2000. Vol. 216. No. 1–4. Pp. 192–203.

14. **Kalaev V. V., Lukanin D. P., Zabelin V. A., Makarov Y. N., Virbulis J., Dornberger E., Ammon W. V**. Prediction of bulk defects in CZ Si crystals using 3D unsteady calculations of melt convection // Materials Science in Semiconductor Processing. 2002. Vol. 5. No. 4–5. Pp. 369–373.

15. **Kalaev V. V., Lukanin D. P, Zabelin V. A., Makarov Y. N., Virbulis J., Dornberger E., Ammon W. V.** Calculation of bulk defects in CZ Si growth impact of melt turbulent fluctuations // Journal of Crystal Growth. 2003. Vol. 250. No. 1–2. Pp. 203–208.

16. **Wetzel T., Virbulis J., Muiznieks A., Ammon W. V., Tomzig E., Raming G., Weber M.** Prediction of the growth interface shape in industrial 300 mm CZ Si crystal growth // Journal of Crystal Growth. 2004. Vol. 266. No. 1–3. Pp. 34–39.

17. **Gräbner O., Müller G., Virbulis J., Tomzig E., Ammon W. V.** Effects of various magnetic field configurations on temperature distributions in Czochralski silicon melts // Microelectronic Engineering. 2001. Vol. 56. No. 1–2. Pp. 83–88.

18. **Müller G, Mühe A., Backofen R., Tomzig E., Ammon W. V**. Study of oxygen transport in Czochralski growth of silicon // Microelectronic Engineering. 1999. Vol. 45. No. 2–3. Pp. 135–147.

19. **Borisov D. V., Kalaev V. V.** ILES of melt turbulent convection with conjugated heat transfer in the crucible and gas flow for Czochralski silicon crystal growth system // Journal of Crystal Growth. 2021. Vol. 573. 1 November. P. 126305.

20. Программный пакет CGSim [Электронный ресурс]. URL: http://www.str-soft.com/products/CGSim/ (Дата обращения: 29.03.2022).

21. **Wolfshtein M.** The velocity and temperature distribution in one-dimensional flow with turbulence augmentation and pressure gradient // International Journal of Heat and Mass Transfer. 1969. Vol. 12. No. 3. Pp. 301–318.

22. **Chien K.-Y.** Predictions of channel and boundary-layer flows with a low-Reynolds number turbulence model // American Institute of Aeronautics & Astronautics (AIAA) Journal. 1982. Vol. 20. No. 1. Pp. 33–38.

23. **Kalaev V., Sattler A., Kadinski L.** Crystal twisting in Cz Si growth // Journal of Crystal Growth. 2015. Vol. 413. 1 March. Pp. 12–16.

24. **Ristorcelli J. R., Lumley J. L.** A second-order turbulence simulation of the Czochralski crystal growth melt: the buoyantly driven flow // Journal of Crystal Growth.1993. Vol. 129. No. 1–2. Pp. 249–265.

25. **Kalaev V., Borisov D., Smirnov A.** A modified hypothesis of Reynolds stress tensor modeling for mixed turbulent convection in crystal growth // Journal of Crystal Growth. 2022. Vol. 580. 15 February. P. 126464.

THE AUTHORS

BORISOV Dmitry V.
STR Group, Inc. – Soft-Impact, Ltd.
64, Bolshoi Sampsonievskii Ave., St. Petersburg, 194044, Russia
dmitriy.borisov@str-soft.com
ORCID: 0000-0002-7481-8265

KALAEV Vladimir V.
STR Group, Inc. - Soft-Impact, Ltd.
64, Bolshoi Sampsonievskii Ave., St. Petersburg, 194044, Russia
vladimir.kalaev@str-soft.com
ORCID: 0000-0001-9231-0740

СВЕДЕНИЯ ОБ АВТОРАХ

БОРИСОВ Дмитрий Витальевич – *инженер-программист АО «Группа СТР» – ООО «Софт-Импакт».*
194044, Россия, г. Санкт-Петербург, Большой Сампсониевский пр., 64
dmitriy.borisov@str-soft.com
ORCID: 0000-0002-7481-8265

КАЛАЕВ Владимир Владимирович – *кандидат физико-математических наук, технический директор АО «Группа СТР» – ООО «Софт-Импакт».*
194044, Россия, г. Санкт-Петербург, Большой Сампсониевский пр., 64
vladimir.kalaev@str-soft.com
ORCID: 0000-0001-9231-0740

Received 29.03.2022. Approved after reviewing 30.05.2022. Accepted 30.05.2022.
Статья поступила в редакцию 29.03.2022. Одобрена после рецензирования 30.05.2022. Принята 30.05.2022.